# Modeling and Simulation of the Second-Generation Orion Crew Module Air Bag Landing System

Richard B. Timmers[1]
*ILC Dover LP, Frederica, Delaware, 19946*

Robin C. Hardy[2]
*NASA Langley Research Center, Hampton, Virginia, 23681*

Joseph V. Welch[3]
*ILC Dover LP, Frederica, Delaware, 19946*

**Air bags were evaluated as the landing attenuation system for earth landing of the Orion Crew Module (CM). An important element of the air bag system design process is proper modeling of the proposed configuration to determine if the resulting performance meets requirements. Analysis conducted to date shows that airbags are capable of providing a graceful landing of the CM in nominal and off-nominal conditions such as parachute failure, high horizontal winds, and unfavorable vehicle/ground angle combinations. The efforts presented here surround a second generation of the airbag design developed by ILC Dover, and is based on previous design, analysis, and testing efforts. In order to fully evaluate the second generation air bag design and correlate the dynamic simulations, a series of drop tests were carried out at NASA Langley's Landing and Impact Research (LandIR) facility. The tests consisted of a full-scale set of air bags attached to a full-scale test article representing the Orion Crew Module. The techniques used to collect experimental data, construct the simulations, and make comparisons to experimental data are discussed.**

## I. Introduction

Ground landing of the Orion Crew Module (CM) using landing air bags is studied in this investigation. This body of work primarily surrounds the landing dynamics and performance of a full-scale CM with air bags under various landing scenarios. Three-dimensional, dynamic finite element analyses (FEA) of the landings are compared against corresponding tests carried out at the Landing Impact Research Facility (LandIR) at the NASA Langley Research Center (LaRC) in Hampton, Virginia. The three dimensional computational mechanics tool, LS-DYNA®, available from Livermore Software Technology Corporation, was used to perform the dynamic analysis of the ground landing of the CM's impact attenuating air bag landing system.

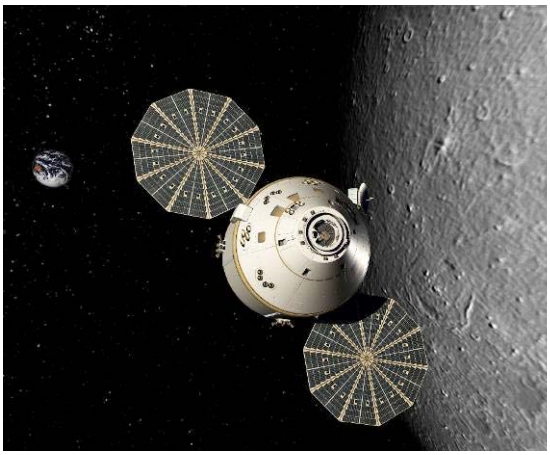

**Figure 1. Artist's rendition of Orion approaching the moon.**

## II. Background

The work presented here is based on the second generation air bag design which was developed following the successful testing of the first generation air bag landing system designed and manufactured by ILC Dover[1-3]. Both the first and second generation air bag systems were developed as part of NASA's Landing System Advanced

[1] Senior Analysis Engineer, One Moonwalker Road, Frederica, DE 19946, AIAA Member
[2] Test Engineer, Structural Dynamics Branch, NASA Langley Research Center Mail Stop 495, Hampton, VA 23681
[3] Lead Analytical Engineer, One Moonwalker Road, Frederica, DE 19946, Senior AIAA Member

Development Project. The testing of the first generation air bag landing system consisted of a half-mass steel weldment boiler plate test article (7300 lbf) with four air bags, half the quantity of the design value of eight. The first generation air bag subassemblies were fixed to the test article using a clamp ring; the test article was instrumented with accelerometers, allowing the landing performance to be compared against simulations. The first generation testing and analysis program showed good correlation between the LS-DYNA models and the experiments, and the air bag design performed well during testing. Thus, the Orion CM air bag landing system matured to the second generation design described here. Instead of the half-mass test article used for the first generation air bag tests, the second generation tests were conducted with a full-scale CM boilerplate which closely represented the dimensions and mass properties of the actual flight CM.

A bag within a bag approach is used in the landing air bag system concept, whereby the outer main air bags, which are vented, provide the primary landing attenuation, while the inner non-vented anti-bottoming air bags provide a lesser contribution to attenuation, but prevent the CM structure from contacting the ground during landing, and provide a stable platform on which the vehicle rests after completion of the landing event. The bag within a bag approach is shown in Fig. 2.

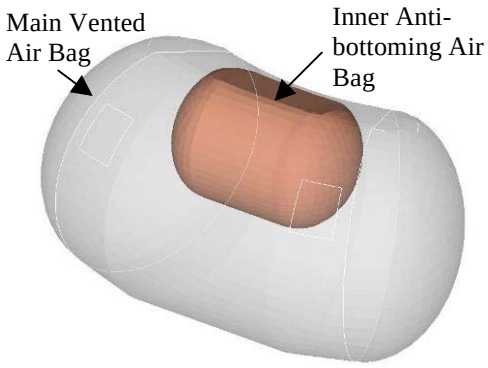


**Figure 2. Bag within a bag configuration**

In the actual CM flight system the air bags would be stowed between the primary heat shield and the aft bulkhead of the CM pressure cabin. The air bags are deployed and inflated after the heat shield is jettisoned. Instead of the eight pairs of air bags (inner and outer) used in the first generation system, a ring of six air bag pairs, each using mitered cylinders, comprised the baseline design for the second generation air bag landing system concept. The air bags are located at the outer circumference of the CM pressure cabin aft bulkhead at the approximate mounting locations shown in Figure 3.

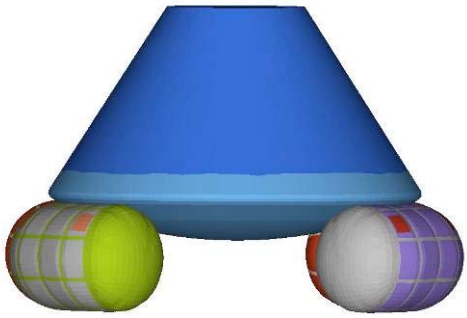

**Figure 3. Air bag locations at the outer circumference of the Crew Module. Two air bags are removed to show the curvature of the CM.**

### A. LS-DYNA Impact Bag Modeling

Initial air bag sizing studies were performed using a one degree-of freedom tool called IMPACT!, which was developed at ILC Dover. IMPACT! results have previously been shown to correlate well with both LS-DYNA predictions and real world test data. ILC Dover uses IMPACT! to rapidly cycle through various combinations of bag size, initial inflation pressure, and orifice venting pressure. After developing an initial configuration, a higher level analysis is performed using LS-DYNA, which includes specific capabilities in the area of modeling landing attenuation air bags.

The explicit finite element code LS-DYNA has been used as the primary tool for conducting detailed dynamic analysis of air bag landing systems. ILC Dover successfully employed impact attenuating air bags to land the Pathfinder, Spirit, and Opportunity Rovers onto Mars. Rockwell, under subcontract to ILC Dover, dynamically modeled the landing event using the LS-DYNA code. In another example, ILC Dover dynamically modeled an air bag landing system for a UAV vehicle using LS-DYNA. A drop test was conducted for the UAV air bag landing system where the results were in good agreement with the LS-DYNA model. In addition, ILC Dover successfully used LS-DYNA to simulate the landing dynamics associated with a first-generation Orion CM air bag design. The results obtained from that study correlated well with physical tests conducted at NASA Langley's LandIR facility[1].

Within LS-DYNA, there are two components that are particularly useful for air bag simulations. The first of these involves the contact between objects with significant differences in material modulus (air bag fabric and the ground) and where thin-walled shell elements (air bag membranes) can result in conditions where the computational contact between the elements can breakdown. The high level treatment of contact in LS-DYNA is needed to overcome these difficulties in air bag landing system modeling. The second advantage of using LS-DYNA for air bag simulations is the control volume capability. This feature is used to model the compressed gas inside the air bag. The element face nodal connectivity of the air bag mesh is used to define the control volume geometry so that nodal displacements and resultant volume are updated in the gas state calculations. Lumped parameter one dimensional flow is included to model the flow of gas into and out of the air bag control volume. Time history data

of the gas state within the control volume are available as output. For landing air bag simulations, the pressure time history is a particularly important output parameter. In addition to being used to evaluate the air bag landing system performance, time history data is also used for model correlation to air bag landing system experiments. The combination of these features in LS-DYNA provides the fundamental building block for air bag landing attenuation simulations.

### B. Air Bag Drop Testing

Different methods of drop testing may be employed depending on the maturity of the landing system product development and the specific test objectives. For the Mars Pathfinder program, drop testing was conducted at NASA Glenn's Plum Brook Station where the Pathfinder air bags and lander were dropped in a vacuum chamber facility to simulate Martian atmospheric pressures. In the Pathfinder test set up, a bungee cord accelerator pulled the lander with about 2000 pounds of force to accelerate it to the desired landing velocity, and then released it when the assembly hit a ground platform.

Helicopter drop tests allow for more of the landing system's components to be fully operational during the experiment. As such, helicopter drops are better suited for the end of the product development process, when many of the individual landing system components have likely gone through their own testing program.

As part of the Landing System Advanced Development Project, the Landing Impact Research Facility (LandIR) at NASA Langley was used to simulate Orion CM ground landing impacts. The LandIR gantry (Figure 4) is a 240 feet high steel truss structure, with heritage dating back to the Apollo program.

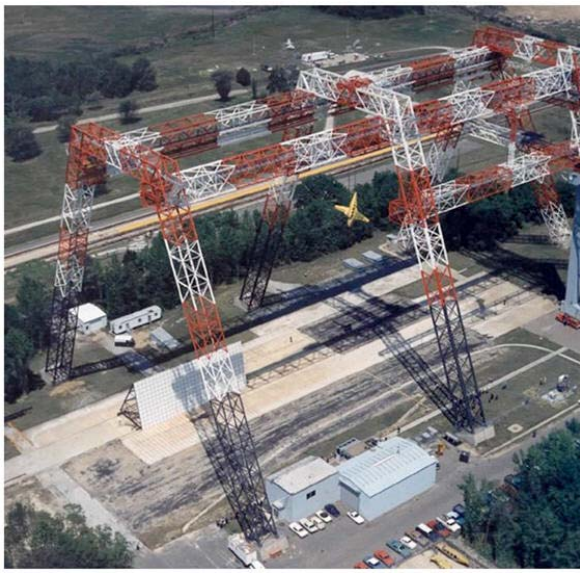

**Figure 4. Landing and Impact Research Facility at NASA Langley**

## III. System Testing

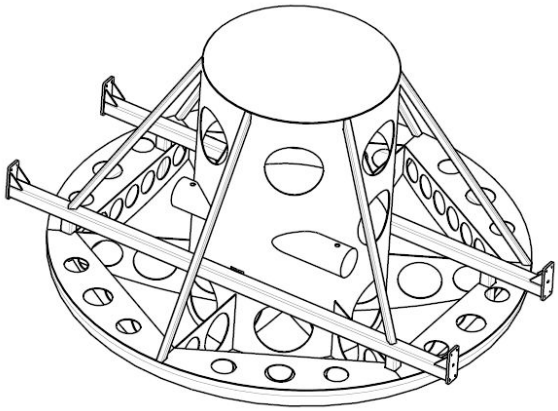

**Figure 5. Air bag test article**

### A. System Test Article Description

As part of the Orion Landing System Advanced Development Project, a second generation air bag test program was completed at NASA Langley's LandIR facility. The objectives for this test program were to validate LS-DYNA analytical models and demonstrate the performance of ILC Dover's second generation airbag design. Various landing scenarios were explored, some only with vertical velocity, and other swing tests that had vertical and horizontal velocity components. In addition, several cases with "toe in" and "heel in" pitch angles were tested. All drop tests used a full-scale boilerplate test article of the Orion CM. Figure 5 shows the geometry of the test article without air bags and Figure 6 provides a view of the test article with the second generation air bags.

The BP4 (boiler plate #4) test article was fabricated by NASA LaRC to represent the mass properties of the Design Analysis Cycle-1 (DAC-1) Orion CM design. The complete structure was fabricated with steel and is a fully welded assembly. The forebody is an off-the-shelf steel dish that was manufactured with a radius of curvature similar to the CM design without the heat shield. The proper center of gravity location is provided by lead ballast that is placed in a pipe. The amount and position of the lead was adjusted to move the CG to the specified position. A support frame was welded to the test article to allow lifting and to provide a means of support when resting on the stand. As the test article needed to be secured in an upright position for safe attachment and inspection of the airbags, a stand was fabricated at the same time as the BP4. In addition, the stand provided a means to support the test article as it was transported to the test location (Figure 7).

**Figure 6. Air bag test article with six air bags**

A simple inflation system using a portable air compressor was designed and fabricated by NASA LaRC to inflate the bags prior to each test. The system being developed for the Orion vehicle includes nitrogen stored at high pressure, control valves, pressure sensors, and associated piping to inflate the each bag. To facilitate testing and allow technicians to readily establish the proper inflation pressure, a simple low pressure system was used. The supply hose connected to a manifold that delivers air to each bag via a pressure regulator. The regulator to each bag is adjusted to maintain the inflation pressure for each main and anti-bottoming bag. To insure that inflation pressures were maintained up to the time of ground impact, the supply hose remained attached to the rear of the test article. Leaving the small hose attached during the landing event had no effect on the dynamic behavior of the test article and was never damaged during a test.

### B. Impact Testing Techniques

Steel cables suspended from the LandIR gantry are utilized to raise Orion drop models to predetermined heights. The models are then dropped to the simulated dry lakebed surface below. Two different types of drop test have been conducted for models with airbags: (1) straight vertical drops, and (2) pendulum-style swing drops. For vertical drop tests, two cables attached to the test article cross beams are connected together to a single cable for lifting. The test article is raised to the proper height for the desired vertical impact velocity. The length of the cables attached to the test article can be used to adjust the pitch or yaw angle. A remotely activated mechanical release hook is used to drop the test article.

In the pendulum style swing tests, six cables are attached to the test article: four swing cables and the two pullback cables (Figure 7). The two pullback cables are connected to a spreader bar which is pulled back with a single cable to the proper initial position for the test. The four swing cables are configured to be parallel to each other. Each swing cable is secured on one end to a winch mounted precisely on the North and South ends of the Western gantry support 'bent' and on the other to the end of a test article cross beam. The initial drop height of the test article and the length of the swing cables determine the vertical and horizontal impact velocities. The lengths of the swing cables can also be adjusted for the

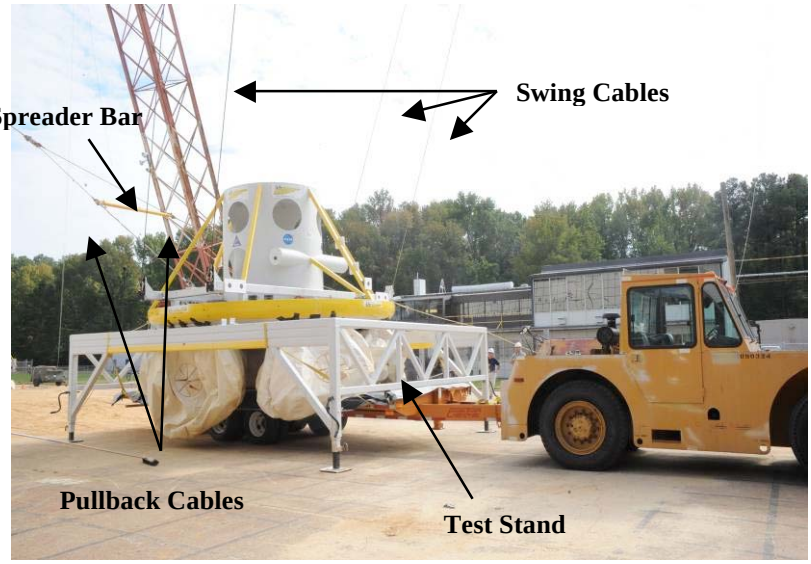

**Figure 7. Test Article as is it is lifted from the Test Stand**

appropriate pitch and yaw attitude at impact. All of the attached cables have explosive wire cutters which are fired in a predetermined sequence to allow the test article to complete the impact and landing event in a free-fall condition. All cutters are electrically shorted prior to arming to prevent them from firing prematurely. The first cutters are triggered remotely to sever the pullback cables connecting the spreader bar to the test article and thereby releasing the suspended Orion model to begin swinging on the four parallel swing cables. Nylon restraint ropes prevent the spreader bar from traveling too far off the gantry centerline. An arming lanyard secured on the spreader bar connects to the swing cable arming pins located on the test article. A second firing lanyard is secured to the East of the test article with weights at a predetermined distance from the impact point. As the test article swings West ward, the lanyard on the spreader bar is pulled taught pulling the arming pins and readying the swing cable cutters to fire. Within a few milliseconds of ground contact, the firing lanyard pulls the firing pins on the swing cable cutters releasing the test article into free fall. The model then has full freedom to continue through the remainder of the test without tether.

### C. Instrumentation and Data Collection

In order to gather data to assess landing performance and draw correlations to finite element simulations, the test article was instrumented to record data throughout the landing tests as shown via a top view of the test article in Figure 8.

Two DAS3200L data collection boxes (32 channels each) manufactured by EME Corporation were used to collect and record to non-volatile memory the outputs from the onboard instrumentation. The DAS3200L, powered by a 10 Volt battery, was able to be controlled remotely via a host PC/AT computer through an Ethernet 10BaseT connection at 3 Mbaud/s thus preventing interference with the natural impact behavior of the test article. A single sample rate of 50,000 at 10KHz was utilized to capture the nuances of the impact. The data output from the DAS3200L was not filtered.

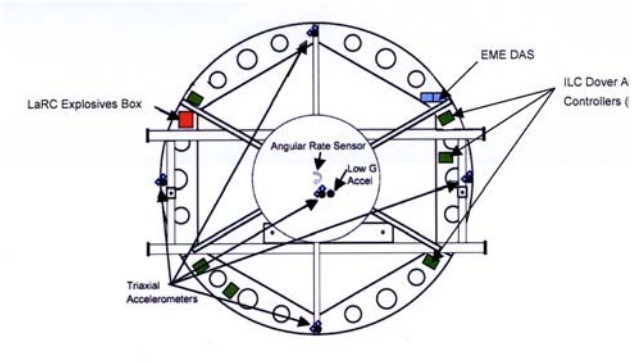


**Figure 8. Top view of Test Article**

'Tri-axial' accelerometers (a block with 3 accelerometers in the x, y and z axes of the test article) were located on the outboard structure at 90° increments as well as at the test article's geometric center. Three additional degrees-of-freedom were measured at the center via an angular rate sensor (tri-axial MEMS gyroscope). Pressure transducers provided by the testing team at NASA LaRC measured and recorded pressures in each of the six inner and outer airbags. The pressure transducers used to control airbag venting were provided by ILC Dover and not recorded on the EME due to concerns of signal interference. The airbag explosive cutter firing signals were recorded as well as data from load cells mounted on several of the straps encompassing the airbags. Finally, an Inter-Range Instrumentation Group (IRIG) time code signal recording at 100 pulses per second was recorded by the EME DAS as a means for correlating the DAS and high speed video data. All instrumentation was calibrated prior to testing using internationally recognized standards traceable to the International System of Units (SI Units). Traceability is achieved through calibrations by the National Institute of Standards and Technology (NIST).

### D. Video and Photogrammetry

Non-intrusive optical measurement techniques were also utilized in the data collection process to measure the spatial position of discrete targets on the CEV models to provide time-histories of displacement, velocity, and model angles. By triangulating from known camera positions to the locations of identical targets on different cameras, photogrammetry provides a time history of the test article position, velocities and rates. Two-dimensional analyses of the drop model impact dynamics within the swing plane were sufficient for analytical model development and validation since temporal identification of primary impact dynamics features, such as initial impact, attitude change, first bounce, etc. was deemed to be more important than obtaining high accuracy spatial values of those events. The

model trajectory and impact data required could therefore be obtained using views from individual high-speed video cameras placed perpendicular to the drop model swing plane.

Five Vision Research, Inc. Phantom high-speed video cameras were utilized to record the images at 1000 frames per second to provide a high resolution visual record of the movement of targets mounted on the test article. Diffuse white dots on a black background are used as the contrast afforded by these targets made automated frame-by-frame tracking reliable, although tracking of discrete targets was occasionally disrupted when the view of a target was obstructed by guide wires, tether ropes, or dust that was kicked up on impact. A combination of Phantom series 7 and series 9 cameras were used.

All cameras were temporally synchronized and simultaneously triggered to begin video acquisition. Three cameras are typically placed perpendicular to the pendulum drop swing plane to capture side views of the test article throughout the drop test. These cameras are designated as North / South cameras to denote the camera viewing directions. From these cameras came the majority of photogrammetry data output. In particular, the Phantom 9 South camera provided vertical and horizontal velocity at impact, average horizontal and vertical velocity, resultant velocity, maximum vertical and horizontal velocities just after ground contact, pitch angle at impact, change in pitch angle, and rate of pitch angle change. Two additional cameras positioned within the swing plane record video from the front (model swinging toward camera) and back (model swinging away from camera) perspectives. These in-plane cameras designated as East / West cameras provide the yaw angle of the vehicle at ground contact as well as the change and rate of change in yaw angle up to ground contact. Each camera was mounted on its own tripod and leveled in two directions with bubble levels. Video was recorded to volatile memory on-board each Phantom camera then downloaded to hard disk at the conclusion of each drop.

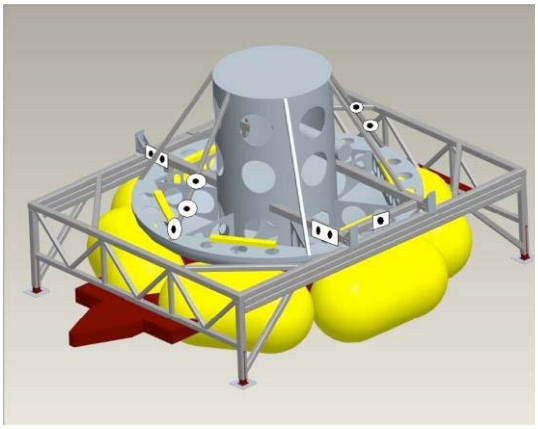

**Figure 9. Test article with photogrammetric targets**

The target centroid locations, having been tracked by the cameras, are converted from image plane pixel units to object plane engineering units by multiplying by the image-to-object plane scaling factor. The target position data were also uniformly shifted in time to set time T = 0 at the point of impact of the test article with the ground typically to within ±2 milliseconds (±2 video frames) by visual inspection of the high-speed video sequences. The time of impact is then correlated to the IRIG Time stamp in order to compare the photogrammetry data to the DAS data. A custom Matlab code was developed to perform the initial manual identification of each photogrammetry target and then to automatically track each target throughout the video sequence.

Trajectory angles are computed using the relative positions of two targets that were on opposite sides of the test article. Computing angles using targets with a large separation distance provides improved measurement accuracy compared to angle measurements using closely spaced targets. Progressing sequentially forward through the video frames, the position of each target within each video frame was determined to ~0.1-pixel accuracy by computing the grayscale-weighted target centroid location.

For post impact travel that was confined to fit in the view of the camera, total slide-out and final resting point were obtained by measuring the distance between the starting and ending locations of targets located parallel to the direction of motion. To ascertain flexing of the test article, actual displacement between targets 1 & 2 is compared with the mean target displacement during flight of the test article as well as over the duration of the test.

The methods employed to extract drop model trajectory and impact data from the high-speed video sequences are based on the principles of single view close-range photogrammetry which assumes that the drop model remains predominantly within the swing plane (minimal out-of-plane motion) and optical system distortions are assumed negligible. Video system optical distortions were minimized through the use of relatively long fixed focal length 35-mm format lenses normally used for high-quality film cameras. Perspective distortion was minimized by carefully aligning the cameras perpendicular to the swing plane. During impact events where out of plane motion was apparent, all of the above data could not be reliably obtained.

### E. Soil Characterization

Designs for energy attenuating systems are dependent on the response characteristics of the impact surface. To that end, material characterization testing of the 2 ft deep soil impact surface was typically conducted following each airbag test. Testing included static and dynamic penetrometer tests using different shapes and masses and friction

testing of the airbag material on gantry soil. Data was also collected on the density of the soil, ambient temperature, and surface moisture content. Four to five drops were conducted using an 8-inch diameter ball penetrometer for each airbag test (Figure 10). Released from a pre-determined height, the penetrometer impacts the contact surface at 12.7 ft/s. An Instrumented Sensor Technology (IST) EDR3 data acquisition system mounted inside the hemisphere records the accelerations in the penetrometer normal and in-plane to the impact surface.

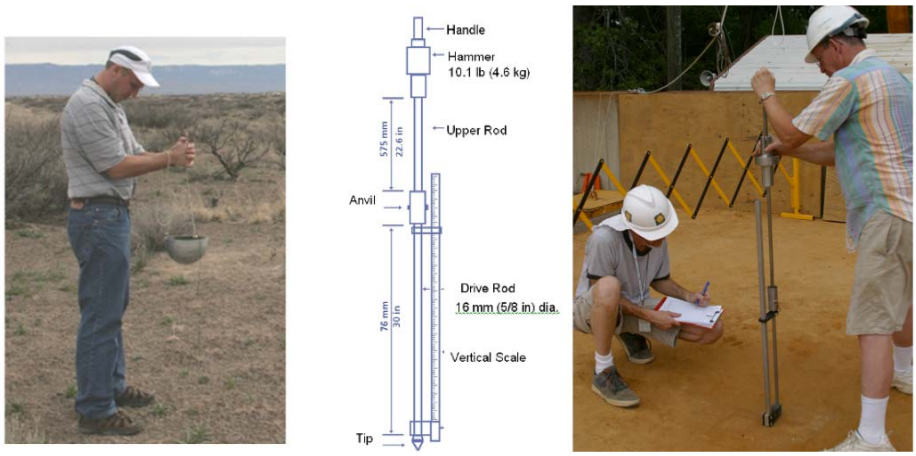


**Figure 10. 20 lb Ball Penetrometer (left and center) and Dynamic Cone Penetrometer (right)**

Three tests using a second device, the Kessler Dynamic Cone Penetrometer (DCP) Model 100, were performed following each airbag test as a means to assess the shear strength and bearing capacity of the impact surface (Figure 10). For both ball and cone penetrometer tests, impact sites selected were at least 12 inches (300 mm) apart to minimize error caused by disturbance of the soil. The DCP device is operated in a vertical position with the tip initially seated such that the top of the widest part of the tip is flush with the surface of the soil. An initial reading is obtained from the vertical scale. The operator then lifts the sliding hammer until it just touches the handle then releases it to free-fall and impact the anvil coupler assembly driving the tip into the soil. For the second generation airbag tests, the tip penetration every three blows was measured and recorded in mm until the tip impacted the concrete floor of the soil bed. The relative compaction of the soil through the depth was determined by comparing penetration rates. Although the calculation was not performed for this test series, the penetration rate can also be used to estimate CBR (California Bearing Ratio).

Soil moisture was measured following each test by taking a soil sample at the impact location. The 'wet' sample was weighed then baked in a 350 deg oven until the water in the soil evaporated, then re-weighed. Soil moisture was calculated by comparing the weight of the soil before and after baking:

% Moisture = (weight wet soil – weight dry soil)/(weight dry soil) X 100

## III. Analysis Methodology

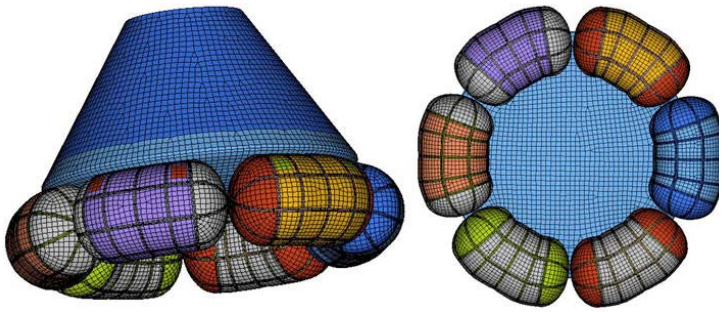

**Figure 11. Side and bottom views of the finite element mesh**

### A. Model Construction

The second generation air bag design uses a bag-in-a-bag approach, comprised of a main (outer) air bag and an anti-bottoming (inner) air bag. Both types of air bags are contained inside a net of 2 inch wide webbing straps. To ensure the inertial landing loads are transferred into the webbing material rather than the air bag fabric, these webbings were foreshortened by one percent in length relative to the air bag geometry. This causes the air bag fabric between slightly bulge out between

webbing locations when the air bags are inflated. The webbings included in the simulation were modeled as a fabric material and fixed to the rigid body of the vehicle by the CONSTRAINED_EXTRA_NODES option in LS-DYNA.

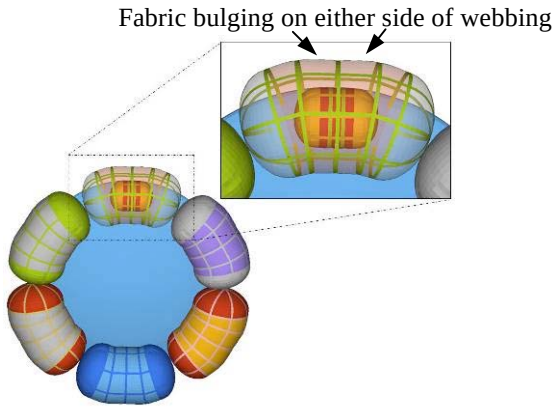


**Figure 12. Bottom view of the model geometry with foreshortened webbing straps. The breakaway image (boxed) provides a view of the bulged fabric between webbing locations due to inflation pressure.**


**Figure 13. Definition of the Main and AB Control Volumes.**


**Figure 14. Air bag position numbering scheme as viewed from above the Crew Module.**

The application eta/VPG developed by Engineering Technology Associates, Inc. was used to produce the mesh for the second generation air bag system geometry. The meshing effort involved two parts: meshing the hardware as a rigid body and meshing the air bag softgoods subassemblies as deformable parts.

The LS-DYNA simulations of the second generation air bag landing system included a representative model of the Orion crew module including the aft bulkhead of the crew compartment which contacts the air bags. The specific geometry of the vehicle was supplied by NASA LaRC.

The crew module was modeled as a rigid body and the air bag softgoods were given deformable material properites. Figure 11 shows the finite element mesh used for the second generation air bag system geometry. As previously noted, the webbing surrounding the main bags was foreshortened by one percent, allowing the inertial taken into the webbings rather than the air bag fabric. This foreshortening strategy was incorporated into the simulations using LS-DYNA's REFERENCE_GEOMETRY card. This option is used regularly in automobile air bag analysis and references an initial nodal position to a final inflated position. The "bulging" effect of the air bag fabric between webbing locations is also observed in the FEA geometry (Figure 12).

The mass properties for the rigid vehicle were not based on the meshed geometry, but rather on an explicit entry of the mass property terms and the center of gravity location into the PART_INERTIA card in LS-DYNA. The translational mass and other components to the inertia tensor were provided by NASA LaRC in the associated Statement of Work.

The air bag fabric and webbing material are the only deformable structures in the LS-DYNA models. The LS-DYNA material model MAT_FABRIC is used with the compressive stress elimination option invoked. A linear elastic liner was also used to analytically define the fabric material. A fully integrated Belytschko-Tsay membrane formulation was assigned to the elements.

Both the webbing and the air bag fabric were modeled as isotropic linear-elastic materials. The elastic properties of the air bag fabric were obtained through uniaxial tensile testing in both the warp and fill directions. Since the material model used in the analysis is isotropic, an average modulus of the two directions was used for the load range of interest.

Contact definitions were required for main air bag to ground, main air bag to test article, main air bag to inner anti-bottoming air bag, webbing to air bag, and webbing to ground interfaces. To accomplish this, several contact models were used: AUTOMATIC_SURFACE_TO_SURFACE_CONTACT was used for air bag contact with the ground/crew module and AIRBAG_SINGLE_SURFACE_CONTACT was used for air bag/webbing self-contact. A small increase in contact thickness, which is a numerical increase in the thickness of a shell element, was used to avoid breakdown of the contact algorithm associated with contact penetrations. The technique of increasing contact thickness is fairly common when modeling a thin material such as the air bags' fabric and is part of the contact callout, leaving the true material thickness unaffected.

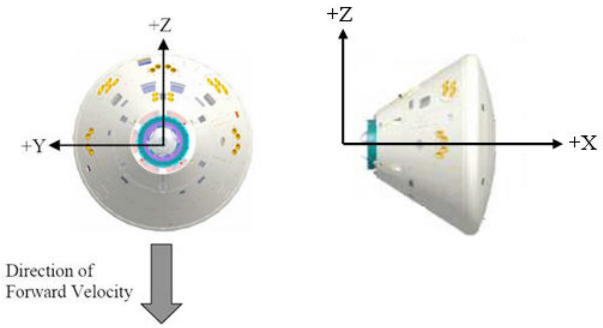


**Figure 15. Local coordinate system for the Orion Crew Module**

The analytical soil surface used for the landing simluations was charcterized by LS-DYNA's MAT_005 (MAT_SOIL_AND_FOAM) material model. The specific parameters of this material model were recommended by NASA LaRC and are appropriate for the unwashed sand that was used at the gantry for the air bag drop tests. The input parameters were derived from a testing effort carried out on the gantry soil by NASA and Applied Research Associates, and provided to ILC Dover in a report by Thomas, Chitty, et al[4].

The AIRBAG_WANG_NEFSKE and AIRBAG_WANG_NEFSKE_POP cards in LS-DYNA were used to model the control volume of compressed gas within the physical air bag structure. The key inputs needed for the CEV landing bag model were:

- Thermo-physical properties of the inflation gas
- Area and orifice coefficient for the air bag vent
- Ambient conditions
- Vent pressure for initiating exit flow through vent
- Time delay before initiating exit flow

A definition of the control volume geometry is needed for the calculations. The control volumes for the air bags as well as the numbering scheme used for their position on the vehicle are shown in Figures 13 and 14. A coordinate system was defined to discuss the angular orientation of the vehicle, as well as the velocity vectors associated with the dynamic landing. This coordinate system is shown in Figure 15.

### B. Orifice Coefficient

There is a great deal of published data on the orifice coefficient, or coefficient of discharge, $C_d$, of machined hardware sharp edge orifices. As part of the first generation air bag test program, a vent test was conducted to better understand this needed input for the LS-DYNA models[2]. Information gained from this exercise was also used in the second generation landing simulations as the vent geometry and surrounding fabric were similar. In the first generation air bag vent test, the inner anti-bottoming air bags were deflated by vacuum to eliminate them from affecting the test. The main air bags where inflated to the design inflation pressure, with active pressure transducers incorporated into the air bags. The vents were signaled to open and the pressure decay on the main bag was monitored. An LS-DYNA model, consisting only of a main air bag was developed to compare with the test results.

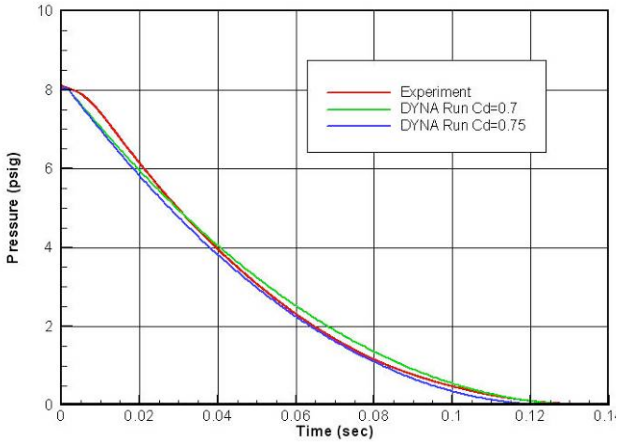


**Figure 16. Pressure discharge curves obtained during the orifice coefficient study.**

Two LS-DYNA options are available for $C_d$, one uses a constant $C_d$ value and the other allows for the $C_d$ value to

vary with time. Since the parameters that affect the orifice coefficient would be expected to vary in an unpredictable manner throughout a given landing event, the option to specify $C_d$ versus time was not practical. The experimental vent test data was therefore compared with results from the air bag only LS-DYNA model assuming different values for a constant $C_d$. The results showed that a constant $C_d$ in the range 0.7 to 0.75 was in general agreement with the experimental data. A value of 0.75 was, therefore, used for the LS DYNA air bag simulations discussed in this report. The associated curves are shown in Figure 16.

### C. Time Delay Associated with Air Bag Venting

The design of the second generation air bag landing system uses main (outer) air bags that are vented to atmosphere at a predetermined pressure. This allows the vehicle to avoid rebounding off of the main air bags for a smoother, more stable landing than would occur if air bags without vents were used. Pressure transducers are in each main bag to monitor the air bag's internal pressure. When the pressure in the air bag reaches the design venting pressure, a pyrotechnic cutter is fired, the vent petals are released, and the internal gas is vented.

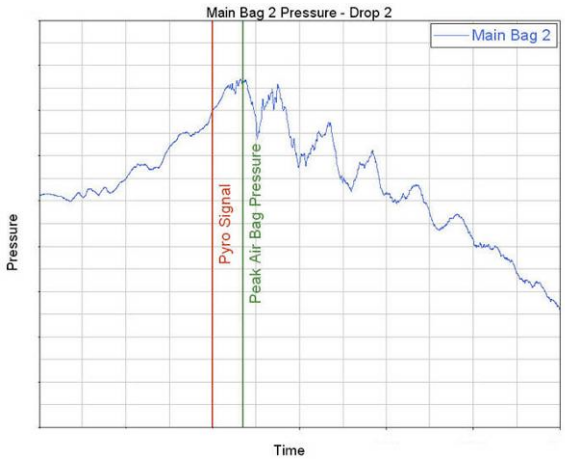


**Figure 17. Typical pressure vs. time plot for a main air bag showing the location of the pyro fire signal and resultant offset.**

A very short time delay was expected between the time the signal is initiated to open the vent and the time at which the vent area is fully open. The delay is caused both by the electronic circuitry and also by the vent itself, in that the vent petals require a minimum amount of time to swing away from the vent opening after being released by the pyrotechnic cutter. Some rough estimates were made to calculate this time delay, but the second generation air bag test program provided actual data that could be used to more accurately quantify the time delay. In the initial second generation drop tests, it was noted that there was a short time delay between the time that the signal was initiated to open the vent, and the time at which there is a significant change in the slope of the main air bag pressure time history. The value of this time delay was estimated at 0.007 seconds. Figure 17 shows a typical pressure plot from the main air bag taken at Bag Station 2, from Test 2 along with the pyro fire signal and the resultant 0.007 second offset. The time delay value was implemented using the TDA option on the AIRBAG_WANG_NEFSKE card, helping the model to better reflect test conditions for the air bag landing system drop tests.

## IV. Model and Experiment Time History Data

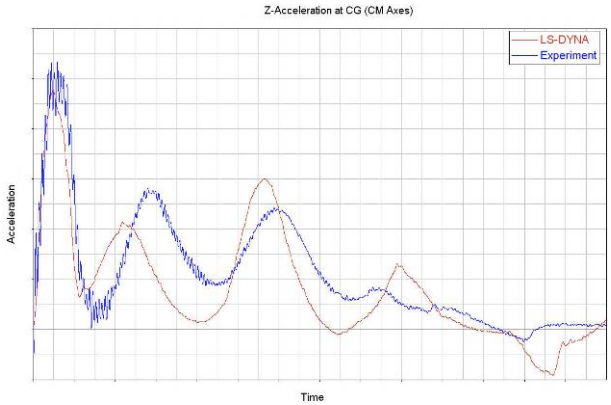


**Figure 18. Experiment/simulation comparison of z-axis (horizontal) acceleration.**

### A. Acceleration and Pressure Comparisons

Seven ILC Dover second generation air bag tests were conducted with various horizontal velocities and pitch angles. The experimental data (e.g. accelerations, air bag pressures) from these tests were in the form of time histories provided to ILC Dover by NASA LaRC. The experimental time history data shown in this report was shifted along the time scale so that it could be compared against output from the LS DYNA simulations; the amount of shift necessary was determined by a visual estimate of the plotted main bag pressure and vertical acceleration data.

Some experimental parameters differed slightly from their intended target conditions. That is, the horizontal and vertical velocities were somewhat higher or lower than the exact values prescribed in the test plan, although within a reasonable range.

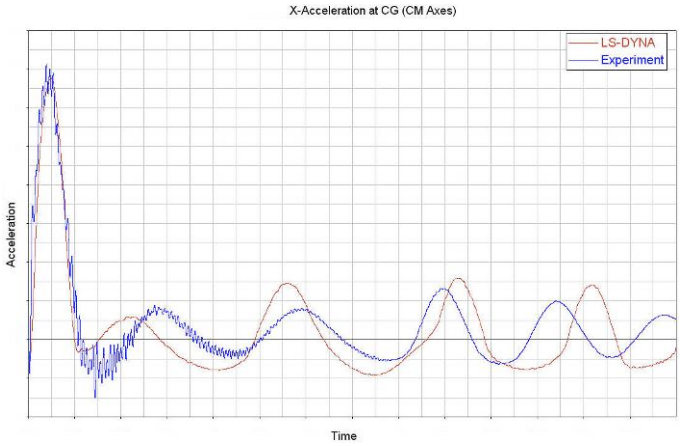


**Figure 19. Experiment/simulation comparison of x-axis (vertical) acceleration**

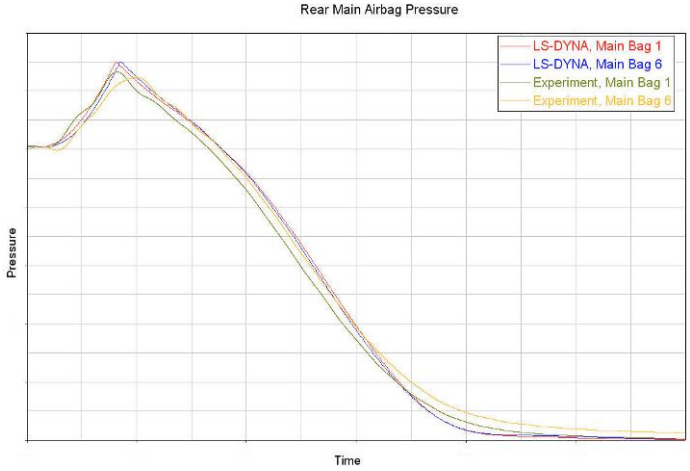


**Figure 20. Experiment/simulation comparison of rear main air bag pressure.**

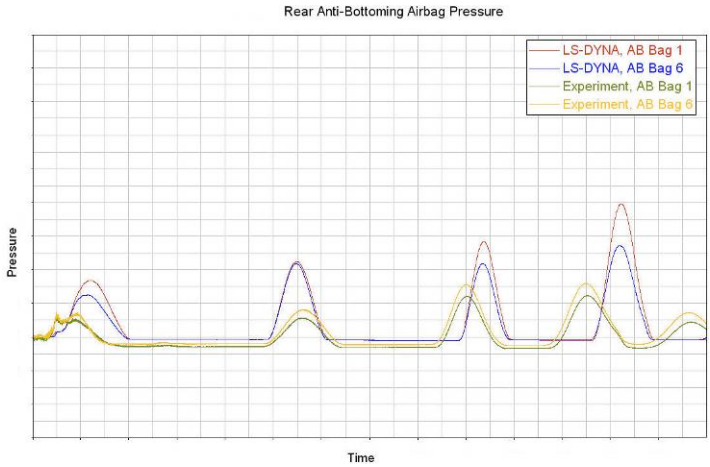


**Figure 21. Experiment/simulation comparison of rear anti-bottoming air bag pressure.**

Acceleration and main air bag pressure test data were treated with a low-pass filter with a cutoff frequency of 70 Hz. The acceleration data obtained from LS-DYNA output was also treated with the same low pass filter, while the LS-DYNA pressure data were not treated with a filter.

Figure 18 gives a similar comparison for the z-axis (horizontal) acceleration at the vehicle's CG associated with a landing which has a horizontal velocity component. Although the experimental data is somewhat noisy, the simulation's prediction of the main horizontal acceleration peak is within 10% of the experimental value. The model's time location of the maxima and minima of the z-acceleration time history also agrees well with the experimental data, as well as the general envelope of deceleration to the point of zero g's.

Figure 19 shows a comparison between the experimental data and simulation results for x-axis (vertical) acceleration at the CG of the Crew Module. The LS-DYNA simulation gives an excellent prediction of the main ground impact peak, within 2% of the experimental value. The subsequent peaks associated with the settling of the vehicle into a stationary position are also well-matched. The phase, or time location, of the maxima and minima in the x-acceleration time history predicted buy the simulation are also in agreement with the experiment.

In addition to horizontal and vertical landing accelerations, the pressure inside the main and anti-bottoming air bags was monitored during the dynamic landing. This was done to verify that main air bag venting was occurring at the appropriate pressure, and that the pressure loads inside the bag did not challenge the ultimate tensile strength of the air bag fabric. The pressure time histories obtained from the experiment were compared against the predictions given from the corresponding simulation.

Figure 20 shows a comparison between the experimental data and simulation for the rear main air bag pressure. The main air bag pressure time histories for the front and side locations are quite similar in terms of shape, venting characteristics, and correlation level with the corresponding model. In the case presented in Figure 20, a good match is observed between the simulation and experimental data, with the model's peak pressure residing within 3% of the

experimental value for Air Bag Position 1 and with 5% for Air Bag Position 6. Both the initial rise in pressure and venting behavior of the main bag is well predicted by the simulation.

Figure 21 shows a typical comparison between the experimental data and simulation results for the pressure inside the rear anti-bottoming air bags during a dynamic landing. The anti-bottoming air bag pressures at the other air bag locations on the vehicle are similar that those shown here. Strong correlations between experimental data simulation results for AB air bag pressures were among the most difficult parameters to achieve, although all comparisons showed reasonable differences.

### B. Photogrammetric Comparisons

High speed video was taken of the landing events from locations forward, on the right hand and on the left hand side of the test article. The resulting photogrammetry data was then compared with the corresponding LS-DYNA model output.

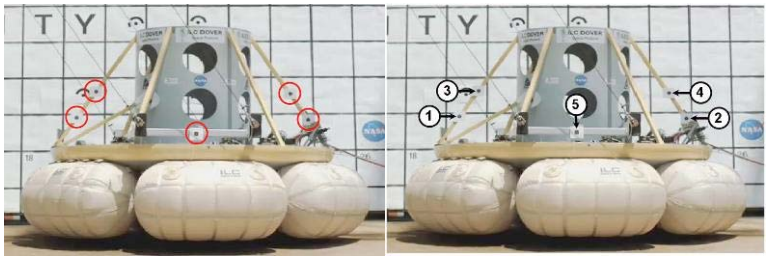


**Figure 22. Orion test article with air bag assemblies attached. Left: Photogrammetric targets are circled in red. Right: Numbering scheme of photogrammetric targets.**

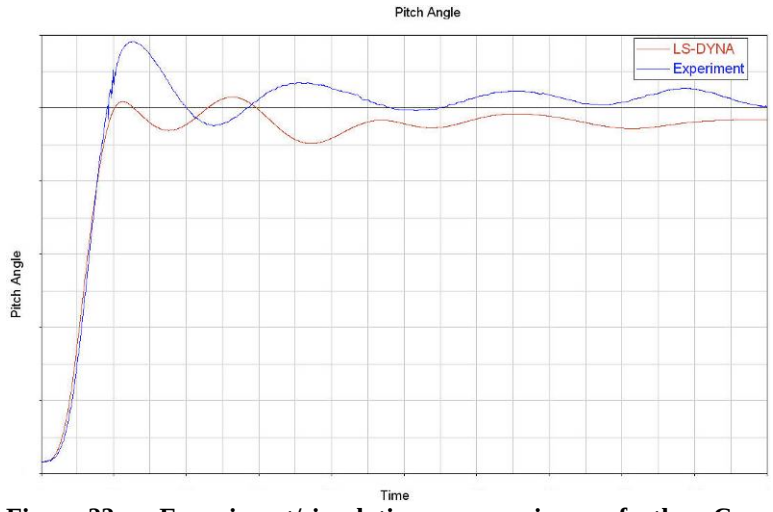


**Figure 23. Experiment/simulation comparison of the Crew Module's pitch angle after impact.**

Parameters studied were vehicle pitch angle (defined as rotation about the y-axis), rotational velocity, vertical velocity, and horizontal velocity. Additionally, information about the "slide-out distance", or horizontal distance traveled following ground impact was also extracted from the photogrammetric data. The targets placed on the test article were numbered 1-5, with their locations shown on Figure 22. Nodes on the Crew Module's mesh were called out in a node set to have their kinematic data output to a LS-DYNA nodout file. The locations of the nodes used in the comparison were chosen by inspection from viewing the photographs of targets on the test article.

Similar to the acceleration and pressure time history data, the results of the simulations were compared against the experimental photogrammetric results data. Figure 23 shows a typical comparison between the simulation and the experiment for the pitch angle during one of the landings of the test program.

The pitching behavior of the vehicle differs slightly from the experiment, primarily due to the variability in the soil's landing surface. For example, one of the highest pitch angles occurring during the test program occurred when the moisture content of the soil was measured to be the highest and the penetrometer reading showed the soil to be softer than usual. These two parameters are not necessarily mutually exclusive; it is likely the increased moisture content leads to a softer soil. A softer, moister soil would allow for deeper penetration of the air bags into the landing surface, especially for cases with a horizontal velocity component. This deeper penetration would cause a larger pitch angle as the vehicle is more likely to pivot about the front portion impacted into the soil.

Figure 24 shows a typical comparison between the simulation and experiment for y-axis rotational velocity (pitch). The simulation's peak rotational velocity for this comparison was within 14% of the experimental maximum value, even considering the inherent noise in the experimental data. Figure 25 shows a representative comparison for the vertical velocity of the Crew Module during landing. Peak rotational velocity values and the phasing of the local minima and maxima are well-matched in the time history plots. Finally, Figure 26 provides a

comparison for horizontal velocity following ground impact. The simulation provides an excellent comparison for the first half of the landing, and slightly under-predicts the horizontal velocity for the remainder of the slide-out.

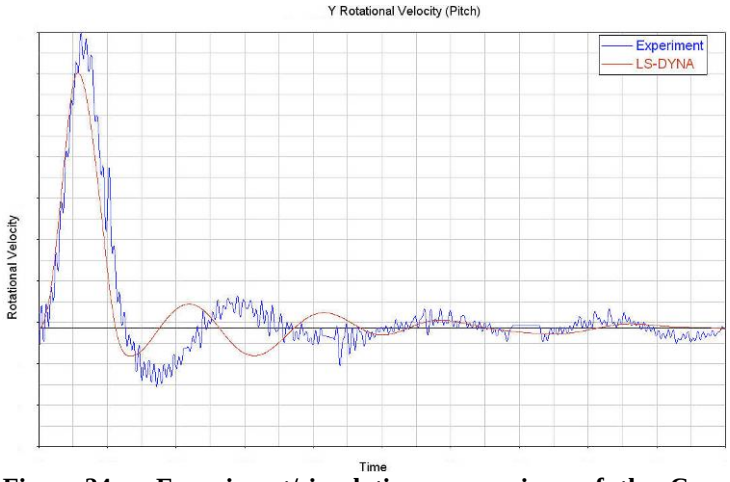


**Figure 24. Experiment/simulation comparison of the Crew Module's rotational velocity after impact.**

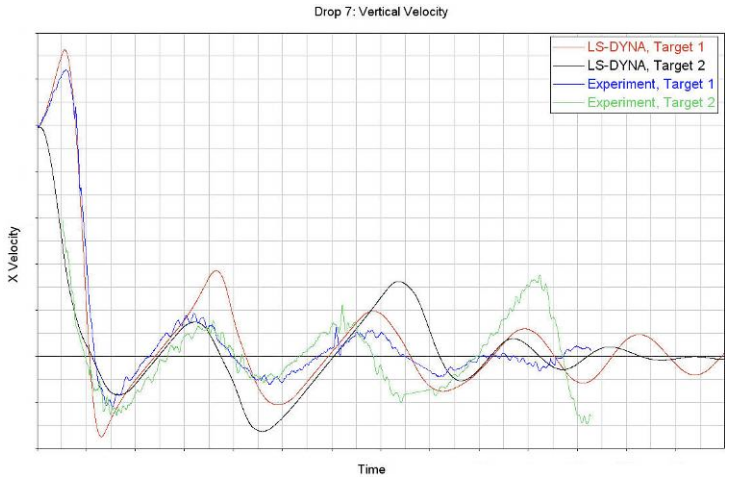


**Figure 25. Experiment/simulation comparison of the Crew Module's vertical velocity after impact.**

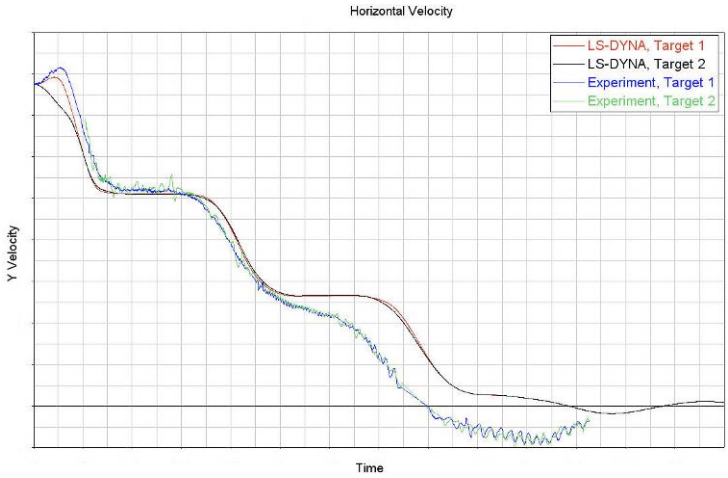


**Figure 25. Experiment/simulation comparison of the Crew Module's horizontal velocity after impact.**

## V. Conclusion

The second generation ILC Dover Orion Crew Module air bag landing system showed outstanding performance during the experimental test program, meeting the requirements outlined by NASA Langley. The work presented in this paper regarding the air bag landing system simulations have produced results which are in good agreement with experimental observations. The drop testing program conducted by NASA as part of the Orion Landing System Advanced Development Project provided valuable information to better understand the LS-DYNA models and the performance of the design of the second generation air bag system. Time history dynamic data and relevant simulation output have been compared for all of the drop test scenarios. This successful LS-DYNA model / experiment comparison provides valuable background for the continued study of the Orion Crew Module air bag landing system, as well as other impact attenuation programs.

## Acknowledgements

The authors would like to thank Jim Corliss, Richard Boitnott, Keith Johnson, and Steve Seider at NASA Langley Research Center, as well as the technical staff at the LaRC LandIR facility.

## References

[1]Shook L., Timmers R., Hinkle J., "Second Generation Airbag Landing System for the Orion Crew Module," *20th AIAA Aerodynamic Decelerator Systems Technology Conference and Seminar*, AIAA, Seattle, WA, 2009, (to be published).

[2]Welch, Joseph V., "CEV Airbag Landing System Generation One Modeling and Testing" NASA Contract No. NNL06AA09B, Task Order NNL06AD11T, October 2007.

[3]Willey, Cliff E., Sandy C., Welch J., and Timmers R., "Impact Attenuating Airbags for Earth and Planetary Landing Systems," AIAA *Space 2007 Conference & Exposition*, AIAA, Long Beach, CA, 2007.

[4]Thomas M.A., Chitty D.E., Gildea M.L., and T'Kindt C.M., "Constitutive Soil Properties for Unwashed Sand at Kennedy Space Center", NASA CR-2008-215334, July 2008.